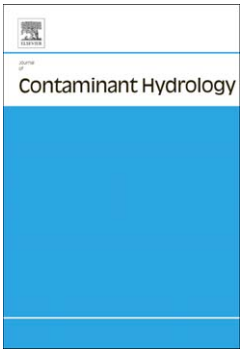

Modelling Colloid Deposition on a Protein Layer Adsorbed to Iron-oxide-coated Sand

X. Yang, R. Flynn, F. von der Kammer, T. Hofmann

PII: S0169-7722(12)00128-3
DOI: doi: 10.1016/j.jconhyd.2012.09.006
Reference: CONHYD 2837

To appear in: *Journal of Contaminant Hydrology*

Received date: 30 January 2012
Revised date: 14 July 2012
Accepted date: 4 September 2012

Please cite this article as: Yang, X., Flynn, R., von der Kammer, F., Hofmann, T., Modelling Colloid Deposition on a Protein Layer Adsorbed to Iron-oxide-coated Sand, *Journal of Contaminant Hydrology* (2012), doi: 10.1016/j.jconhyd.2012.09.006

Modelling Colloid Deposition on a Protein Layer Adsorbed to Iron-oxide-coated Sand

X. Yang[a,b,*], R. Flynn[b], F.von der Kammer[c,], T.Hofmann[c,*]

[a] *Provincial Key Laboratory of Agricultural Environmental Engineering, College of Resources and Environment, Sichuan Agricultural University ,Huimin Road 211, Chengdu, 611130, Sichuan Province, China*

[b] *School of Planning, Architecture & Civil Engineering, Queen's University Belfast, David Keir Building, Stranmillis Road, Belfast, BT9 5AG, UK*

[c] *Department of Environmental Geosciences, University of Vienna, Althanstrasse 14, 1090 Vienna, Austria*

**Corresponding authors:*
X. Yang (yangxinyao@hotmail.com; Tel.: +86-28-86291390; Fax: +86-28-82652669)
T. Hofmann (thilo.hofmann@univie.ac.at; Tel.: +43(1)427753320; Fax: +43(1)42779533)

List of Symbols

A=Column cross section

a_c= Radius of sand grain

C= Colloid effluent concentration

C_e= Initial colloid effluent concentration

C_0= Colloid injection concentration

D=Column inner diameter

D_p=Dispersion coefficient of colloids

d_c= Diameter of sand grain

d_l= Major axis length of BSA (14nm)

d_p= Diameter of colloid

d_s= Minor axis length of BSA (3.8nm)

K_c= Number of end-on BSA directly impacted by a deposited colloid

k_d=Colloid deposition rate

k_r=Colloid release rate

K_1= Number of end-on BSA generated due to one impacted BSA

K_2= Number of end-on BSA shielded by a deposited colloid

L=Column length

N_0= Total number of adsorbed BSA

N_{10}= Number of end-on BSA adsorbed before colloid deposition

$N_1(t)$= Number of end-on BSA adsorbed during colloid deposition

N_{20}= Number of side-on BSA adsorbed before colloid deposition

$N_3(t)$= Number of deposited colloids

$N_c(t)$= Number of end-on BSA occupied by deposited colloids, including the directly impacted and the shielded BSA

$N_s(t)$= Number of colloids deposited directly on the sand surface

N_{max}= Maximum allowable number of side-on BSA adsorbed on a sand grain

$N_{s,max}$= Maximum allowable number of colloids deposited directly on a sand grain

$N(t)$= Number of colloid collectors

Q= Flow rate

S=Deposition density of colloids

v_p= Flow velocity of colloids

α= Collision efficiency of colloid on a sand collector

α_p = Collision efficiency of colloid on a colloid collector

β_1 = Empirical parameter accounting for shadow effect (i.e., the fraction of the collector surface inaccessible to approaching colloids; set to 1/3: Vigneswaran and Tulachan, 1988)

ε=Porosity of column matrix

ε_0=Porosity of column matrix before colloid deposition

ε_u=Limiting porosity corresponding to ultimate deposition condition

η= Single collector efficiency of colloid on a sand grain

η_p = Single collector efficiency of colloid on a colloid collector associated with the sand grain

$\eta_r(t)$=Overall single collector efficiency of colloid ($=\eta + \eta_p$)

ABSTRACT

Our recent study reported that conformation change of granule-associated Bovine Serum Albumin (BSA) may influence the role of the protein controlling colloid deposition in porous media (Flynn et al., 2012). The present study conceptualized the observed phenomena with an ellipsoid morphology model, describing BSA as an ellipsoid taking a side-on or end-on

conformation on granular surface, and identified the following processes: (1) at low adsorbed concentrations, BSA exhibited a side-on conformation blocking colloid deposition; (2) at high adsorbed concentrations, BSA adapted to an end-on conformation promoted colloid deposition; (3) colloid deposition on the BSA layer may progressively generate end-on molecules (sites) by conformation change of side-on BSA, resulting in sustained increasing deposition rates. Generally, the protein layer lowered colloid attenuation by the porous medium, suggesting the overall effect of BSA was inhibitory at the experimental time scale. A mathematical model was developed to interpret the ripening curves. Modelling analysis identified the site generation efficiency of colloid as a control on the ripening rate (declining rate in colloid concentrations), and this efficiency was higher for BSA adsorbed from a more dilute BSA solution.

Keywords: Colloid deposition; granule-associated BSA; side-on conformation; end-on conformation; mathematical modelling.

1. Introduction

Colloids are usually defined as entities with at least one dimension between 1nm and 1μm (IUPAC: McNaught and Wilkinson, 1997). Groundwater colloids may originate locally by mobilization or precipitation, or enter groundwater from external sources such as septic tank effluent, leaky sewer, river bank infiltration, artificial recharge, and anthropogenic

nanomaterials (Kretzschmar et al., 1999; Foppen et al., 2006; Nowack and Bucheli, 2007). The large specific surface areas of colloids make them potentially important sorbents and vehicles of environmental contaminants, which may include heavy metals, radionuclides and hydrophobic organic compounds (Hofmann and Wendelborn, 2007; Bekhit et al., 2009). Meanwhile, certain colloid types such as pathogenic microorganisms and engineered nanoparticles may themselves constitute intrinsic hazard to human health (Levy et al., 2007; Mueller and Nowack, 2008). Thus, understanding the key controls on colloid transport in porous medium is important for better groundwater protection.

Protein is a major organic compound widespread in wastewater-impacted groundwater (Harrison, 2001; Imai et al., 2002; Tchobanoglous et al., 2003). Published studies have reported the contrasting influence protein may have on colloid mobility (Weber-Shirk, 2002; Kuznar and Elimelech, 2005; Kim et al., 2009). Weber-Shirk (2002) found that a low adsorbed protein mass (acid-soluble seston extract, $<1.2 g/m^2$) may substantially increase colloid attenuation by porous medium. Conversely, Kuznar and Elimelech (2005) and Kim et al. (2009) noted that the protein expression in a bacteria surface may inhibit the colloid deposition. Several authors noted that conformation change may cause a redistribution of the surface adsorbing property of a protein and influence its interaction with solid phases (Urano and Fukuzaki, 2000; Bhattacharjee et al., 2000). The outcome of these studies implies that protein adsorption conformation might be controlling the function of protein on colloid deposition. On the other hand, protein conformation was universally recognized to be influenced by its adsorption concentration (density) (Urano and Fukuzaki, 2000; Nakanishi et

al., 2001; Stutz, 2009). Our recent study conducted with distinct protein adsorption concentrations showed that a single type of protein, Bovine Serum Albumin (BSA), may act either as colloid deposition site or inhibitor, depending on the adsorbed conformation (Flynn et al., 2012). This reconciles the conflicting responses observed in previous studies. However, lack of a suitable ripening model for describing the influence of a protein adsorption layer restricted our previous study solely to quantifying the site blockage by BSA, while the fundamental processes driving the ripening phenomenon remain unclear.

This study aims to address this research gap by developing a mathematical model and applying the model to further explore the ripening process. As a prerequisite for model development, a conceptualization of the observed processes needs to be established, utilizing a widely accepted ellipsoid morphology BSA model for analyzing the experimental results. This conceptual model permits the mathematical formulation of the ripening process to be achieved based on a modification of existing filter ripening models, developed for organic matter-free pure colloid deposition systems.

2. Double Pulse Column Experiments (DPEs)

Materials: With the exception of the organic matter (protein), all materials and apparatus employed in column experiments were the same as those employed by Yang et al. (2010). Fluoresbrite® yellow-green fluorescent stained polystyrene latex microspheres (microspheres) with carboxylic functional groups and a nominal diameter of 0.2 µm (Polysciences Inc.,

Eppelheim, Germany) were used as model colloid. Microsphere suspension was prepared and dispersed ultrasonically in the same way as described in Yang et al. (2010) (See Supplement).

Bovine Serum Albumin (BSA) (Acros Organics, Geel, Belgium), a model of wastewater protein (Ang and Elimelech, 2007), was investigated. The molecule is flexible and amorphous, consisted of amino acids and peptide bonds (Nakanishi et al., 2001; Rogalinski et al., 2005) and has an isoelectric point of approximately pH4.7 (Chiku et al., 2008). There is a consensus that surface properties of BSA vary across the molecule giving rise to charge heterogeneity (Baier et al., 2011), along with hydrophobic and hydrophilic regions (Yoon et al., 1998). Consequently, morphological models of BSA needs simplification to certain degrees: it is described either as a globular ellipsoid of about 14 x 3.8 x 3.8 nm (Ke et al., 2009; Togashi et al., 2009), a heart-shaped solid with three different domains (Voros, 2004), or a flexible foldable polymer (Chiku et al., 2008). Among them, the ellipsoid model not only provides explicit size and geometry description of the protein molecule, but also offers a realistic means to characterise the adsorbed conformation in end-on (long axis perpendicular to collector surface) or side-on (short axis perpendicular to collector surface) (Yoon et al., 2003; Schrott et al., 2009). This renders the globular ellipsoid model well suited for this study. In this study, BSA levels in column effluent were measured online by HPLC UV-vis spectrophotometer (VWD) (Agilent 1100 Series, Waldbronn, Germany) set at 230 nm.

Methods: Double pulse column experiments (DPEs: see Table 1) all consisted of a prolonged pulse of multiple pore volumes (PV) of BSA at contrasting concentrations, succeeded by flush

with microsphere-free/BSA-free electrolyte solution, and a second 13 PV pulse of microsphere dispersion at 10.4 ppm (2.5×10^9 colloids mL^{-1}), followed by a final flush with microsphere-free/BSA-free electrolyte solution. The BSA pulse, injected for variable durations, aims to produce a BSA layer of distinct adsorption concentrations and consequently different BSA conformations on the granular surface. Employing a range of injection BSA concentrations permitted the influence of the suspending concentration on the property of the adsorbed protein layer to be evaluated.

Based on the injected BSA masses, the DPEs fall into two groups. The first group consisted of three DPEs, injecting a BSA mass of 1.2×10^{-9} mole (DPE A), 3×10^{-10} mole (DPE B), and 6×10^{-10} mole (DPE C), respectively. The approach permitted characterisation of the general trend in microsphere response to different levels of BSA adsorption concentrations where low masses of BSA were adsorbed. In a similar manner, a second group of DPEs consisted of three experiments, injecting 1.2×10^{-7} mole (DPE D), 3×10^{-8} mole (DPE E), and 7.5×10^{-9} mole BSA (DPE F). This series of experiments aimed to characterize the functional relationship between microsphere responses and high BSA adsorption concentrations. In addition to these experiments, a separate series of experiments were conducted, using only a microsphere tracer without any addition of BSA, to directly compare the effects of BSA. All the experiments were carried out in triplicate.

3. Experimental Results and Discussions

3.1. Double Pulse Column Experiment (DPE) Results

Figure 1 summarises the results of DPEs (DPE A, DPE B, DPE C) employing low BSA concentrations. Breakthrough curves (BTCs) reveal that no BSA was detected in the column effluent, suggesting nearly complete attenuation of BSA by the column matrix. Table 1 lists the adsorbed BSA concentrations calculated by averaging the total BSA mass adsorbed in the column matrix over the overall surface area of the column sand, assuming sand grain to be spherical with a mean diameter of 125 µm. The adsorbed BSA mass declined in the order of DPE A>DPE C> DPE B. The succeeding microsphere BTCs in DPE A, DPE B, and DPE C display similar shapes: microsphere relative concentrations initially rose rapidly, before reaching a point of inflection, and following that point, concentrations rose at lower rates. By comparison, the height of the inflection point decreases in the order of DPE A (22%)> DPE C (12%)> DPE B (8%). No notable tailing was observed in these microsphere BTCs.

Figure 2 summarises the results of DPEs using high BSA input concentrations (DPE D, DPE E, DPE F). The BSA effluent concentrations all reached significantly high levels, developing an inflection point at 86% in DPE F and at 100% in DPE D and DPE E within less than 5 PVs. Microsphere BTCs show that particle effluent concentrations in DPE D (36%), DPE E (48%) and DPE F (57%) all reached an inflection point higher than those displayed in low BSA experiments, followed by transition to a phase of declining microsphere

concentrations. This BTC shape contrasts sharply with the rising phase observed in DPEs employing low BSA levels (DPE A, DPE B, DPE C).

Figure 3 compares the time series of adsorbed BSA concentrations (in the unit of mg/m^2) and the BSA breakthrough curves for the three DPEs employing high BSA. The BSA adsorption concentration curve indicates that the breakthrough started when similar amount of BSA was adsorbed: $2.8mg/m^2$ in DPE F and $3.1mg/m^2$ in DPE D and DPE E.

3.2. BSA Adsorption Conformation

Rapid BSA recovery from column matrix (Figure 2) suggests that the adsorbed BSA may inhibit further adsorption. Kretzschmar et al. (1999) stated that a BTC exhibiting this feature is a strong symbol of monolayer deposition. The finding that BSA did not adsorb in multilayer is consistent with other studies (i.e. Su et al., 1998; Tencer et al., 2007).

It is widely accepted that when adsorbed, BSA may first take a side-on conformation, at low adsorbed concentrations, which then change gradually to an end-on conformation, as more BSA masses adsorbed and lateral repulsion between adjacent BSA molecules became significant (Ramsden, 1995; Nakanishi et al., 2001; Stutz, 2009). In the absence of direct observation, the conformation of an adsorbed BSA could be estimated by comparing the adsorbed concentration with the limiting values proposed for a full side-on BSA layer and for a full end-on BSA layer, respectively (Revilla et al. 1996; Nakanishi et al. 2001; Terashima and Tsuji 2003; Tencer et al. 2007; Togashi et al. 2009: see Figure 4). Calculation results suggest that all the experiments injecting low mass BSA (DPE A, DPE B, and DPE C) had

adsorbed protein concentrations less than the low limits cited in literature, while all those injecting high mass BSA (DPE D, DPE E, and DPE F) had adsorbed BSA concentrations between the low and high limits (see Table1 and Figure 4). According to the above criteria, this suggests an incomplete layer of side-on BSA in DPE A, DPE B, and DPE C, and a full layer consisting of end-on and side-on BSA molecules in DPE D, DPE E, and DPE F.

Additional evidence supporting the above speculation on the BSA adsorption conformation may be gained by a comparison between the BSA BTC data and the BSA adsorption concentration curve for the high BSA experiments (DPE D, DPE E and DPE F) (see Figure 3). The good correspondence of the starting point of colloid breakthrough with the point where the adsorbed BSA concentrations significantly exceeded the cited maximum possible adsorption concentration for a full side-on BSA layer (see Figures 3 and 4) consistently suggests that before saturating the sand grain, BSA adsorbed side-on at a high rate resulting in 100% BSA attenuation. Following saturation of the collector surface by side-on BSA where further adsorption may induce conformation change from side-on to end-on (See Figures 3 and 4) , BSA adsorption occurred at rapidly declining rates, resulting in abrupt rise in BSA effluent concentrations. This was probably due to the increasing resistance from the adsorbed protein layer which had growing adsorption concentrations. Such a two stage BSA adsorption process was noted also by other researchers (i.e., Nakanishi et al., 2001). The consistency in the BSA adsorption concentration and breakthrough concentration data thus further confirms the BSA layer structure as speculated above.

3.3 Influence of BSA on Colloid Deposition

3.3.1. Side-on BSA inhibits colloid deposition

According to Ryan and Elimelech (1996), a higher inflection point on a BTC suggests a lower availability of deposition sites. For the BTC of double microsphere pulse experiment (DPE PC), the higher inflection point developed on the second microsphere pulse BTC (Supplement Figure S3) indicates that fewer number of deposition sites remained due to site coverage by microspheres deposited through the first pulse. Kretzschmar et al. (1995) and Yang et al. (2010) also observed this type of behaviour in multiple pulse column experiments.

Data analysis in the Section 3.2 suggests that for experiments employing low BSA concentrations (DPE A, DPE B, and DPE C), the BSA may adsorb in a side-on conformation and the resulting BSA adsorption layer may not have saturated the granular surface. For all these experiments, an inflection point in the microsphere BTC developed at a level comparable to, or higher than the inflection point in the corresponding microsphere BTC observed in BSA-free DPE PC. Absence of significant tailing in the microsphere BTC suggests that the release of the previously deposited microspheres was not a process responsible for the higher microsphere recovery. Consequently, this suggests that the side-on adsorbed BSA also has site coverage effect on microsphere deposition, in a manner akin to the microsphere deposited in the first pulse of DPE PC. Flynn et al. (2012) quantified the site blockage by BSA utilizing the dynamic blocking model of Johnson and Elimelech (1995).

3.3.2. End-on BSA promotes colloid deposition

Surface coverage calculations reported earlier suggested that in high BSA experiments (DPE D, DPE E, and DPE F), a full layer of BSA with both end-on and side-on conformations developed on the collector surface. Despite the site saturation by BSA, as reflected by relative BSA concentrations reaching unity in BTCs, microsphere deposition rates following the BSA adsorption remained significant, as indicated by the inflection points (36%-57%) in the microsphere BTC (Figure 4). Analysis of microsphere BTCs of DPEs employing lower BSA concentrations (DPE A, DPE B and DPE C) has suggested that when BSA adsorbed with a side-on conformation, it covered microsphere deposition sites and inhibited the deposition. As a corollary to this point, microsphere deposition in DPE D, DPE E, and DPE F probably occurred on the end-on BSA molecules. Our previous zeta potential measurement of a solution containing both BSA and microsphere indicated that favourable regions occurring in BSA permitted its adsorption to microsphere. Moreover, we found that the sand-associated molecule upon compaction might expose its attractive regions for microsphere deposition. (Flynn et al., 2012). Similar findings had been reported by Xu and Logan (2005) who stated that conformation change may alter the nature and magnitude of surface interaction forces exerted by BSA, a soft flexible molecule with heterogeneous distribution of contrasting adsorption properties (e.g., hydrophobic regions and negatively charged functional groups). The present study further identified it was the end-on conformation that rendered the BSA capable of adsorbing microspheres. However, the high BSA DPEs generally had a lower initial deposition rate than the low BSA DPEs, probably due to the co-occurring side-on BSA

in the protein layer. Flynn et al. (2012) has quantified the site blockage by the side-on components in this type of protein layers.

The gradual decline in column effluent concentrations observed in experimental BTCs reflects the matrix's increasing microsphere attenuation capacity as further microspheres were deposited. Previous studies conducted in organic matter-free systems normally attributed this phenomenon to multilayer colloid deposition driven by the attractive colloid-colloid interactions and called it filter ripening (Kretzschmar et al., 1999; Kuhnen et al., 2000). However, gradual rise in microsphere concentrations, shown in BSA-free systems, i.e., DPE PC, indicates that microsphere interaction was dominated by repulsion, not attraction. Zeta potential and size measurement also suggested that high electrostatic repulsion operating between microspheres prevented aggregation (Flynn et al., 2012). Moreover, since BSA had been injected separately from and before the microsphere pulse, surface modification of suspending microspheres by BSA adsorption was not an expected case either. Consequently, the observed ripening must be driven by other factors not present in BSA-free experiments, i.e. being a result of BSA adsorption on sand surface.

Sustained increase in the number of favourable colloid deposition sites is a precondition for ripening to occur (Kuhnen et al., 2000; Kulkarni et al., 2005). Experimental analysis above implies that end-on BSA may function as microsphere deposition sites. Ramsden (1995) and Stutz (2009) noted that end-on BSA may be generated by conformation change of side-on BSA, under the action of lateral compression. Our previous study suggested that deposition of

microspheres onto the compactly adsorbed protein generated new protein surfaces that further enhanced colloidal deposition rates (Flynn et al., 2012). This study shows that the process could be explained using the ellipsoid morphology BSA model as follows: microsphere deposition may induce lateral expansion of the impacted molecule, which in turn compress the adjacent side-on BSA to end-on conformation, resulting in a growing number of end-on BSA while more microspheres deposited (see Figure 5 and Supplement for schematic illustration and animation of this process). Despite the ripening process, inflection points of the microsphere BTCs all reached higher altitudes in high BSA DPEs (D-F) indicating the overall effect of the adsorbed protein was inhibitory to microsphere deposition at the experimental scale (see Table 1).

4. Modelling Transient Colloid Deposition on BSA-amended Granular Surface

Based on the conceptual model established through experimental analysis, a mathematical model was developed and applied to interpret the BSA-induced ripening phenomenon in this Section.

4.1. Model Development

Under steady state flow conditions, transport of colloidal particles through granular porous media can be described by a convective-dispersive transport equation including terms to account for colloid deposition and release (de Marsily, 1986).

$$\partial C/\partial t = D_p(\partial^2 C/\partial x^2) - v_p(\partial C/\partial x) - (\rho_b/\varepsilon)(\partial S/\partial t) \quad (1)$$

$$(\rho_b/\varepsilon)(\partial S/\partial t) = k_d C - (\rho_b/\varepsilon)k_r S \quad (2)$$

When colloid release is negligible, the transport equation can be simplified to the following (Kretzschmar et al., 1999):

$$\partial C/\partial t = D_p(\partial^2 C/\partial x^2) - v_p(\partial C/\partial x) - k_d C \quad (3)$$

k_d is the deposition rate related to the single collector efficiency (η) by the following expression (Elimelech et al., 1995):

$$k_d = \frac{3}{2}\frac{(1-\varepsilon)}{d_c}\eta v_p \quad (4)$$

Substituting Equation (4) into Equation (3) yields:

$$\frac{\partial C}{\partial t} = D_p\frac{\partial^2 C}{\partial x^2} - v_p\frac{\partial C}{\partial x} - \frac{3}{2}\frac{(1-\varepsilon)}{d_c}\eta v_p C \quad (5)$$

O'Melia and Ali (1978) stated that for a small volume of filter bed, the mass balance equation could be simplified to:

$$\frac{\partial C}{\partial t} = -v_p\frac{\partial C}{\partial x} - \frac{3}{2}\frac{(1-\varepsilon)}{d_c}\eta v_p C \quad (6)$$

Considering η and C as step functions of time, then for a discrete time step, the variation in particle concentration with time ($\partial C/\partial t$) can be neglected, yielding a solution as follow

(O'Melia and Ali,1978; Vigneswaran and Tulachan, 1988; Tobiason and Vigneswaran, 1994; Adou et al., 2007).

$$\frac{C(i)}{C_0} = \exp\left[-\frac{3}{4}\frac{(1-\varepsilon)}{a_c}\eta(i-1)L\right] \quad (7)$$

Where $C(i)$ is particle concentration at the i^{th} time step, $\eta(i-1)$ is single collector efficiency for the (i-1) time step, L is the bed thickness. This expression relates the removal efficiency of the whole filter bed (C/C_0) to the removal efficiency of a single granular collector (η). The boundary condition employed for solving Equation (6) was $C=C_0$, (x=0). The initial condition was $C=C_e$ (t=0, x=L), where C_e is the initial effluent concentration shown by the inflection point on the colloid breakthrough curve.

While significant amount of colloids deposit, they would interfere with further deposition, resulting in a variation of deposition rate with time. In presence of attractive colloid interactions, deposition may occur on the pre-deposited particles, forming multiple layers. In this situation, the overall deposition rate would rise gradually, due to the combined effect of particle collectors and sand collectors (Kuhnen et al., 2000; Adou et al., 2007). Adou et al. (2007) shows that the two effects are additive and can be integrated in the following formula calculating the single collector efficiency:

$$\eta_r(t) = \alpha\eta\left[\frac{N_{s,max} - N_s(t)}{N_{s,max}}\right] + N(t)\alpha_p\eta_p\left[\frac{\varepsilon - \varepsilon_u}{\varepsilon_0 - \varepsilon_u}\right]\left(\frac{d_p}{d_c}\right)^2 \quad (8)$$

The first term in Equation (8) states that the deposition rate of particles which directly attach on a sand surface is proportional to the number of favourable sites accessible on the sand collector. This assumption had been employed by other authors (i.e., Johnson and Elimelech, 1995; Ryan and Elimelech, 1996). Similarly, the second term suggests that particle removal by deposited particles is proportional to the available number of the deposited ones. Despite of its wide recognition, application of the Equation to the OM-induced ripening process is questionable, since it was developed without considering the influence of organic matter.

In our study, experimental analysis indicates that BSA had saturated the sand surface ($C/C_0=1$) and the subsequent colloid deposition may have occurred on the BSA layer. Accordingly, the colloid sites on the sand collector (first term of Equation 8) were provided by the end-on BSAs adsorbed on the sand. Dominance of repulsive colloid interactions suggests the absence of colloid collectors, thus the second term in Equation (8) can be removed. These modifications result in the following expression:

$$\eta_r(t) = \frac{\alpha\eta[N_1(t)-N_c(t)]}{N_{10}} \qquad (9)$$

Where $[N_1(t) - N_c(t)]/N_{10}$ is the fraction of end-on BSA available for colloid deposition. The number of available end-on BSA ($N_1(t)$) would increase due to BSA conformation change, under the impact of colloid deposition. On the other hand, the number of end-on BSA occupied by colloids ($N_c(t)$) also increases with colloid deposition. The overall deposition rate thus depends on the interplay of these two counteracting processes. The initial single

collector efficiency ($\alpha\eta$) can be estimated using Equation (10) (Song and Elimelech, 1993; Johnson et al., 1996)

$$\alpha\eta = -\frac{2}{3}\frac{d_c}{(1-\varepsilon)L}\ln\left(\frac{C_e}{C_0}\right) \quad (10)$$

Supposing that each colloid impacts on K_c end-on BSA molecules and that each impacted BSA causes K_1 side-on molecules to adapt to end-on conformation, then the deposited colloids ($N_3(t)$) would generate $N_3(t)K_cK_1$ end-on BSA. Thus, $N_1(t)$ could be expressed as:

$$N_1(t) = N_{10} + N_3(t)K_cK_1 \quad (11)$$

K_1 is a fitting parameter. K_c is a constant determined by the geometry of colloid and BSA (See Figure 8) to be 721in this study.

The initial number of end-on BSA (N_{10}) adsorbed prior to colloid deposition is a constant determined as follow. On the assumption that the total surface coverage by BSA adsorbed on a sand grain equals the total accessible surface area of the grain, a geometric relationship between initial number of end-on BSA (N_{10}) and side-on BSA (N_{20}) is established:

$$N_{10}(\pi d_s^2/4) + N_{20}d_s d_l = \beta_1 \pi d_c^2 \quad (12)$$

Moreover, the total number of BSA (N_0) on one granule is the sum of the end-on (N_{10}) and side-on (N_{10}) BSA molecules.

$$N_0 = N_{10} + N_{20} \quad (13)$$

Substituting Equation (12) into Equation (13) generates the expression of N_{10}:

$$N_{10} = (4N_0 d_s d_l - 4\beta_1 \pi d_c^2)/(4d_s d_l - \pi d_s^2) \quad (14)$$

On the other hand, a deposited colloid may also reduce the number of end-on BSA, by physical impaction and electrostatic blocking via double layer forces (see Figure 6).The double layer blocking effect of a deposited colloid has been well established (i.e., Johnson and Elimelech, 1995; Ko and Elimelech, 2000).

Supposing that the number of end-on BSA impacted and blocked per deposited colloid is K_c and K_2, respectively, then the total number of end-on BSA made unavailable by the deposited colloids ($N_3(t)$) is:

$$N_c(t) = N_3(t)(K_c + K_2) \quad (15)$$

Substituting Equations (11) and (15) into Equation (9) yields the expression for the overall single collector efficiency:

$$\eta_r(t) = \alpha\eta[1 + (N_3(t)/N_{10})(K_1 K_c - K_2 - K_c)] \quad (16)$$

Integration of the model generated colloid breakthrough curve permits the number of colloids deposited on one sand granule ($N_3(t)$) to be calculated:

$$N_3(t) = \frac{\pi d_c^2 [C_0 Q \int_0^t (1 - C(t)/C_0) dt]}{6AL(1-\varepsilon)} \quad (17)$$

The maximum possible deposition density of spherical particles on a spherical collector can be calculated by dividing the total collector surface area by the cross section of the particle

(Vigneswaran and Tulachan, 1988). Similarly, the maximum allowable number of BSA molecules, all adsorbed in side-on conformation, on one sand grain, may be calculated as:

$$N_{max} = (\beta_1 \pi d_c^2)/(d_s d_l) \quad (18)$$

While $N_0 < N_{max}$, all BSA molecules adsorb side-on and inhibit colloid deposition. In this situation, filter ripening may not occur.

While $N_0 > N_{max}$, BSA over-saturates the site such that a fraction of side-on BSA adapts to end-on conformation. Colloid deposition on the protein layer may generate ripening.

Model simulation starts by loading the measured BSA breakthrough data, based on which the total number of BSA molecules adsorbed (N_0) by a granular collector is calculated. If this value is higher than the maximum possible amount for a full side-on protein layer (N_{max}), estimated by Equation (18), Equation (14) is employed to estimate the number of end-on BSA (N_{10}) occurring before colloid deposition. This permits the initial condition of the protein layer to be modelled. During the colloid deposition phase, Equation (17) is employed to calculate the number of colloids deposited at a time step, which is then substituted into Equation (16) to estimate an updated single collector efficiency. Substitution of the collector efficiency into Equation (7) permits the colloid concentration for the next time step to be calculated. In this recursive manner, the synchronized processes of colloid deposition and BSA conformation change could be simulated, generating a colloid effluent concentration at every time step.

4.2 Model Parameter Evaluation

K_1 and K_2 are two fitting parameters characterizing the behavior of the protein layer in response to microsphere deposition. A high K_1 value means a high number of end-on BSA (sites) generated for each impacted molecule, while a high value of K_2 means a high number of end-on BSA deactivated by a deposited microsphere. These parameters are integrated into a term ($K_1K_c - K_c - K_2$) which measures the site generation efficiency of microspheres (net number of end-on BSA generated per deposited microsphere). As the value of K_1 and K_2 is influenced by a series of bio- and physic-chemical conditions including protein structure, conformation & elasticity, particle size & geometry, and solution chemistry, the site generation efficiency term reflects the combined effect of complex environmental conditions. The relationship between this efficiency and microsphere deposition rate is described by Equation (16). Instead of calculating a value for each parameter, the model estimates the total value of the site generation efficiency term by fitting the model output to the ripening section of the measured microsphere BTC.

Figure 7 summarises model-simulated ripening curves for a range of site generation efficiencies. Results show that ripening rate (the rate of declining concentrations) increases with increasing site generation efficiencies, i.e. at a $K_1K_c - K_c - K_2$ value of 2159 and 10815, the relative concentrations declined by 8.3% and 32% over 18 PVs, respectively. A negative site generation efficiency, i.e., -5, means that the deactivated sites, by each deposited microsphere, exceed the generated. Under such circumstance, the process of microsphere

deposition results in a gradual decreasing sites, incurring the gradual rise in microsphere concentrations.

4.3. Simulating Ripening Phenomenon & Quantification

Figure 8 summarises the model simulated ripening curves, which display a high consistency with the experimental data. A fitting to the experimental ripening curve permitted the values of site generation efficiency and single collector efficiency to be quantified (Table 2). Mass balance calculation based on the BSA BTC shows that comparable number of BSA molecules adsorbed on a sand grain among the three experiments, that is, $1.85\pm0.02 \times 10^{9}$, $1.95\pm0.25 \times 10^{9}$, and $1.77\pm0.05 \times 10^{9}$ molecules for DPE D, DPE E, and DPE F, respectively. Nevertheless, experimental colloid BTC data reveals a notably greater decline in relative effluent concentration (of 7.5±0.5%) in DPE F, in comparison to the 2.4±0.5% decline in DPE D and DPE E, over the 13 pore volume colloid pulse. Model calculation shows that such a magnitude of decline corresponds to about 27% rise in single collector efficiency in DPEs D and E and 37% rise in DPE F (Table 2). This suggests that in spite of the comparable amount of BSA adsorbed, they demonstrated different capability on promoting colloid deposition: ripening rate was higher in DPE F than in DPE D and DPE E. Model parameter evaluation conducted in Section 4.2 shows that ripening is enhanced at higher site generation efficiency. A comparison of the values of the site generation efficiency and percentage rise in single collector efficiency (Table 2), calculated by the model for the experimental data, suggests the similar trend.

It is interesting to note that the BSA layer adsorbed from an identical injection concentration has comparable capacity changing colloid deposition rates, i.e. DPE D and DPE E. Conversely, even that comparable number of BSA molecules adsorbed, the protein layer resulting from a higher BSA injection concentration (DPE D and DPE E) displayed lower deposition-promoting efficiency. Previous AFM study by Sheller et al. (1998) showed that the bulk solution concentration of BSA may influence the morphology of adsorbed protein layers. Further study to establish the relationship between solution concentration and adsorbed protein structure &surface properties will shed more light on the fundamental mechanisms driving the transient protein and colloid processes observed in this study.

5. Conclusion and Environmental Implications

This study is an extension of our recent work which reported the paradox colloid responses to a protein layer of distinct packing densities (Flynn et al., 2012). In the present work, it is demonstrated that the observed phenomena could be interpreted with an ellipsoid morphology BSA model, based on which we found that the site blocking was due to the side-on conformation of BSA while the end-on BSA acted as colloid deposition sites. The BSA-induced ‘filter ripening’ was attributed to a continuous generation of end-on BSA, due to the colloid depositing on the protein layer, which in turn resulted in progressive enhancement in colloid deposition rates. On the other hand, despite the concentration-induced colloid responses contrast with our previous work on humic acid (HA) adsorption (Yang et al., 2010, Yang et al., 2011), which showed HA blocked colloidal desposition at all the

investigated adsorption concentrations, the overall effect of the protein layer was similar to humic acid, i.e., lowering microsphere attenuation by the porous medium. A more recent study by us on EDTA showed that the synthetic organic ligand could also enhance colloid mobility, but by eluting the colloid sites (Yang et al., 2012). The outcome of these series of studies highlighted the mobility-enhancing mechanisms may be organic matter-type specific and the need to further investigate the influential mechanisms of other environmentally relevant organic matter types in order to better understand the fate and transport of colloids in heterogeneous field environments.

A mathematical model was developed to simulate the conceptualized ripening phenomenon. Modelling analysis suggested that the ripening rate is related to the site generation efficiency of a depositing microsphere, or the net number of end-on molecules generated per deposited microsphere. The bulk solution concentration of BSA has been identified as an factor influencing the value of site generation efficiency: at comparable adsorption concentrations, BSA adsorbed from more concentrated solutions demonstrated a lower efficiency promoting colloid deposition. Further study to investigate other environmental factors controlling the site generation efficiency of a depositing particle, i.e., particle size, solution pH and ionic strength, and BSA properties, can definitely deepen the understanding of the BSA-induced 'ripening' process. The model developed in this study could be used as a supporting tool.

The protein concentrations employed correspond well to the levels of typical relatively undiluted wastewaters reported in Raunkjær et al. (1994), and when it has undergone

(forty-fold) dilution with protein free water. Study findings are expected to have implications to colloid transport phenomena in wastewater-impacted groundwater systems.

Acknowledgements

This work was supported by the Natural Science Foundation of China (Grant No.: 41101475) and the Special Research Scholarship of Queen's University Belfast.

Table of Figure Captions

Figure 1 Representative double pulse experimental breakthrough curves with BSA and Microspheres (error within ±2.5%). Note that the microsphere injection pulse was identical. While the injected BSA concentrations and pore volumes were as follows: (A) DPE A: 10^{-7}M BSA for 13PVs. (B) DPE B: 10^{-7}M BSA for 3PVs. (C) DPE C: $2x10^{-7}$M BSA for 3 PVs. The error range shows standard deviation (Data from Yang, 2010, PhD Dissertation).

Figure 2 Representative double pulse experimental breakthrough curves (error within ±2.5%). Note that the microsphere injection pulse was identical. While the injected BSA concentrations and pore volumes were as follows: (D) DPE D: $4x10^{-6}$M BSA for 32PVs. (E) DPE E: $4x10^{-6}$M BSA for 8PVs. (F) DPE F: 10^{-6}M BSA for 8PVs. The error range shows standard deviation (Data from Yang, 2010, PhD Dissertation).

Figure 3 BSA breakthrough curves and adsorption concentration curves for Double Pulses Experiments (DPEs): DPE D (up), DPE E (middle), and DPE F (bottom). The adsorbed BSA concentration was calculated by averaging the overall BSA adsorbed over the total column sand surface area. The error range shows standard deviation.

Figure 4 Maximum possible adsorption concentrations for a full BSA adsorption layer on a spherical collector in side-on conformation (left), blended side-on and end-on conformations (middle), and end-on conformation (right). (Data cited from Revilla et al., 1996; Nakanishi et al. 2001; Terashima and Tsuji, 2003; Tencer et al., 2007; Togashi et al., 2009).

Figure 5 Schematic illustration of colloid deposition on BSA adsorption layer to interpret the respective colloid breakthrough curves: Left---Deposition on an incomplete side-on BSA layer involves the following processes: irreversible deposition on sand (IA), deposition blocked (inhibited) by side-on BSA (BB), and deposition blocked by deposited colloids (BC). Right---Deposition on a full BSA layer of side-on and end-on conformations involves the following processes: irreversible deposition on end-on BSA (IA) inducing protein

deformation and consequent conformation change of side-on BSA to end-on, deposition blocked by side-on BSA (BB), and deposition blocked by deposited colloids (BC).

Figure 6 Schematic illustration of the geometrical relationship employed in the mathematical model to calculate the total number of end-on BSA (K_c) impacted by a deposited colloid. Note that all the end-on BSA molecules adsorbed within a circular zone with radius $\sqrt{a_p^2-(a_p-d_1)^2}$ were impacted.

Figure 7 Evaluating the influence of site generation efficiency ($K_1K_c-K_c-K_2$) on the ripening rate. The higher the generation efficiency, the higher the ripening rate. Modelling parameters: L=0.03m, D=0.01m, d_c=125μm, d_p=0.2μm, U=7.2m/Day, $\eta_r(0)$ =0.0047, ε=0.39, $N_0=4\times10^8$ BSA.

Figure 8 Model fitting of the ripening section of colloid BTCs for double pulse column experiments. Model parameter ($K_1K_c-K_c-K_2$) are 1.12±0.01×10^4, 1.35±0.02 ×10^4, and 2.01±0.02 ×10^4 for DPE D, DPE E, and DPE F, respectively.

Table of Table Captions

Table1 List of Double Pulse Column Experiments and Adsorbed Masses

Table 2 Model Parameters & Results

Reference

Adou, Y.A.F., Muhandiki, V.S., Shimizu, Y., Matsui, S., 2007.Experimental and modeling investigations of wastewater filtration. Desalination 202, 182-190.

Alkan, M., Demirbas, O., Dogan, M., Arslan, O., 2006. Surface properties of bovine serum albumin-adsorbed oxides: adsorption, adsorption kinetics and electrokinetic properties. Microporous and Mesoporous Materials 96, 331-340.

Ang, W.S., Elimelech, M., 2007. Protein (BSA) fouling of reverse osmosis membranes: Implications for wastewater reclamation. Journal of Membrane Science 296, 83-92.

Baier, G., Costa, C., Zeller, A., Baumann, D., Sayer, C., Araujo, P.H.H., Mailänder, V., Musyanovych, A., Landfester, K., 2011. BSA adsorption on differently charged polystyrene nanoparticles using isothermal titration calorimetry and the influence on cellular uptake. Macromolecular Bioscience 11, 628-638.

Bekhit, H.M., Ei-Kordy, M.A., Hassan, A.E. 2009. Contaminant transport in groundwater in the presence of colloids and bacteria: Model development and verification. Journal of Contaminant Hydrology 108,152-167.

Bhattacharjee, S., Chen, J.Y., Elimelech, M., 2000. DLVO interaction energy between spheroidal particles and a flat surface. Colloids Surf. Physicochem. Eng. Aspects 165, 143-156.

Chiku, M., Nakamura, J., Fujishima, A., Einaga, Y., 2008. Conformational change detection in nonmetal proteins by direct electrochemical oxidation using diamond electrodes. Analytical Chemistry 80, 5783-5787.

de Marsily,G., 1986. Quantitative hydrogeology: groundwater hydrology for engineers. Academic Press, New York.

Elimelech, M., Gregory, J., Jia, X., Williams, R., 1995. Particle deposition and aggregation: measurement, modelling and simulation. Butterworth-Heinemann, Oxford.

Flynn, R., Yang, X., Hofmann, T., v.d. Kammer, F., 2012. Bovine serum albumin adsorption to iron-oxide coated sands can change microsphere deposition mechanisms. Environmental Science & Technology 46, 2583-259.

Foppen, J.W.A., Okletey, S., Schijven, J.F., 2006. Effect of goethite coating and humic acid on the transport of bacteriophage PRD1 in columns of saturated sand. Journal of Contaminant Hydrology 85, 287-301.

Harrison, R.M., 2001. Pollution: causes, effects and control. 4th edn. Bookcraft Ltd, UK.

Hofmann, T., Wendelborn, A., 2007. Colloid facilitated transport of polychlorinated dibenzo-p-dioxins and dibenzofurans (PCDD/Fs) to the groundwater at Ma Da area, Vietnam. Environmental Science and Pollution Research 14, 223-224.

Imai, A., Fukushima, T., Matsuhige, K., Kim, Y., Choi, K., 2002. Characterization of dissolved organic matter in effluents from wastewater treatment plants. Water Res. 36, 859-870.

Johnson, R.P., Elimelech, M., 1995. Dynamics of colloid deposition in porous media: blocking based on random sequential adsorption. Langmuir 11, 801-812.

Johnson, R.P., Sun, N., Elimelech, M., 1996. Colloid transport in geochemically heterogeneous porous media: modeling and measurements. Environmental Science Technology 30, 3284-3293.

Ke, X.B., Shao, R.F., Zhu, H.Y., Yuan, Y., Yang, D.J., Ratinac, K.R., Gao, X.P., 2009. Ceramic membranes for separation of proteins and DNA through in situ growth of alumina nanofibres inside porous substrates. Chemical Communications , 1264-1266.

Kim, H.N., Bradford, S.A., Walker, S.L., 2009. Escherichia coli 0157:H7 transport in saturated porous media: role of solution chemistry and surface macromolecules. Environmental Science Technology 43, 4340-4347.

Ko, C., Elimelech, M., 2000. The "shadow effect" in colloid transport and deposition dynamics in granular porous media: measurements and mechanisms. Environmental Science Technology 34, 3681-3689.

Kretzschmar, R., Borkovec, M., Grolimund, D., and Elimelech, M., 1999. Mobile subsurface colloids and their role in contaminant transport. Advances in Agronomy 66, 121-193.

Kretzschmar, R., Wayne, P.R., Aziz, A., 1995. Influence of natural organic matter on colloid transport through saprolite. Water Resources Research 31, 435-445.

Kuhnen, F., Barmettler, K., Bhattachajee, S., Elimelech, M., Kretzschmar, R., 2000. Transport of iron oxide colloids in packed quartz sand media: monolayer and multilayer deposition. Journal of Colloid and Interface Science 231, 32-41.

Kulkarni, P., Sureshkumar, R., Biswas, P., 2005. Hierachical approach to model multilayer colloidal deposition in porous media. Environmental Science Technology 39, 6361-6370.

Kuznar, Z.A., Elimelech, M., 2005. Role of surface proteins in the deposition kinetics of Cryptosporidium parvum Oocysts. Langmuir 21, 710-716.

Levy, J., Sun, K., Findlay, R.H., Farruggia, F.T., Porter, J., Mumy, K.L., Tomaras, J., Tomaras, A., 2007. Transport of escherichia coli bacteria through laboratory columns of glacial-outwash sediments: estimating model parameter values based on sediment characteristics. Journal of Contaminant Hydrology 89,71-106.

McNaught, A.D., Wilkinson, A., 1997. IUPAC. Compendium of Chemical Terminology, in: Anonymous , 2nd ed. Blackwell Scientific Publications, Oxford.

Mueller, C.N., Nowack, B., 2008. Exposure modeling of engineered nanoparticles in the environment. Environmental Science Technology 42, 4447-4453.

Nakanishi, K., Sakiyama, T., Imamura, K., 2001. On the adsorption of proteins on solid surfaces, a common but very complicated phenomenon. Journal of Bioscience and Bioengineering 91, 233-244.

Nowack, B., Bucheli, D.T., 2007. Occurrence, behaviour and effects of nanoparticles in the environment. Environmental Pollution 150, 5-22.

O'Melia, C.R., Ali, W., 1978. The role of retained particles in deep bed filtration. Progress in Water Technology 10, 167-182.

Ramsden, J.J., 1995. Puzzles and paradoxies in protein adsorption. Chemical Society Reviews 24, 73-78.

Raunkjær, K., Hvitved-Jacobsen, T., Halkjær, N.P., 1994. Measurement of pools of protein, carbohydrate and lipid in domestic wastewater. Water Research 28, 251-262.

Revilla, J., Elaissari, A., Carriere, P., Pichot, C., 1996. Adsorption of bovine serum albumin onto polystyrene latex particles bearing saccharidic moieties. Journal of Colloid and Interface Science 180, 405-412.

Rogalinski, T., Herrmann, S., Brunner, G., 2005. Production of amino acids from bovine serum albumin by continuous sub-critical water hydrolysis. Journal of Supercritical Fluids 36, 49-58.

Ryan, N.J., Elimelech, M., 1996. Review: Colloid mobilization and transport in groundwater. Colloids and Surfaces A: Physicochemical and Engineering Aspects 107, 1-56.

Schrott, W., Slouka, Z., Cervenka, P., Ston, J., Nebyla, M., Pribyl, M., Snita, D., 2009. Study on surface properties of PDMS microfluidic chips treated with albumin. Biomicrofluidics 3, 044101-044115.

Sheller, N.B., Petrash, S., Foster, M.D., Tsukruk, V.V., 1998. Atomic force microscopy and X-ray reflectivity studies of albumin adsorbed onto self-assembled monolayers of hexadecyltrichlorosilane. Langmuir 14, 4535-4544.

Song, L., Elimelech, M., 1993. Dynamics of colloid deposition in porous media: modeling the role of retained particles. Coll. Surf. A 73, 49-63.

Stutz, H., 2009. Protein attachment onto silica surfaces - a survey of molecular fundamentals, resulting effects and novel preventive strategies in CE. Electrophoresis 30, 2032-2061.

Su, J.T., Lu, R.J., Thomas, K.R., Cui, F.Z., Penfold, J., 1998. The conformational structure of bovine serum albumin layers adsorbed at the silica-water interface. Journal of Physical Chemistry 102, 8100-8108.

Tchobanoglous, G., Burton, L.F., Stensel, D.H., 2003. Wastewater engineering: treatment and reuse. 2003, 4th ed. McGraw-Hill Higher Education, New York.

Tencer, M., Charbonneau, R., Lahoud, N., Berini, P., 2007. AFM study of BSA adlayers on Au stripes. Applied Surface Science 253, 9209-9214.

Terashima, H., Tsuji, T., 2003. Adsorption of bovine serum albumin onto mica surfaces studied by a direct weighing technique. Colloids and Surfaces B: Biointerfaces 27, 115-122.

Tobiason, J.E., Vigneswaran, S., 1994. Evaluation of a modified model for deep bed filtration. Water Research 28, 335-342.

Togashi, D.M., Ryder, A.G., Heiss, G., 2009. Quantifying adsorbed protein on surfaces using confocal fluorescence microscopy. Colloids and Surfaces B: Biointerfaces 72, 219-229.

Urano, H., Fukuzaki, S., 2000. Conformation of adsorbed bovine serum albumin governing its desorption behavior at alumina-water interfaces. Journal of Bioscience and Bioengineering 90, 105-111.

Vigneswaran, S., Tulachan, R.K., 1988. Mathematical modelling of transient behaviour of deep bed filtration. Water Resource 22, 1093-1100.

Voros, J., 2004. The density and refractive index of adsorbing protein layers. Biophysical Journal 87, 553-561.

Weber-Shirk, M.L., 2002. Enhancing slow sand filter performance with an acid-soluble seston extract. Water Research 36, 4753-4756.

Xu, L.C., Logan, B.E., 2005. Interaction forces between colloids and protein-coated surfaces measured using an atomic force microscope. Environmental Science Technology 39, 3592-3600.

Yang, X., 2010. Influence of natural organic matter on colloid transport and attenuation in saturated porous media- Experimentation and modelling. PhD Dissertation. The Queen's University Belfast July 2010, 1-377.

Yang, X., Flynn, R., v. d. Kammer, F., Hofmann, T., 2010. Quantifying the influence of humic acid adsorption on colloidal microsphere deposition onto iron-oxide-coated sand. Environmental Pollution 158, 3498-3506.

Yang, X., Flynn, R., v. d. Kammer, F., Hofmann, T., 2011. Influence of ionic strength and pH on the limitation of latex microsphere deposition sites on iron-oxide coated sand by humic acid. Environmental Pollution 159, 1896-1904.

Yang, X., Liang, D., Deng, S., 2012. Quantifying the influence of EDTA on polymer nanoparticle deposition and retention in an iron-oxide-coated sand column. Journal of Environmental Monitoring DOI: 10.1039/c2em30145h.

Yoon, J.Y., Lee, J.H., Kim, J.H., Kim, W.S., 1998. Separation of serum proteins with uncoupled microsphere particles in a stirred cell. Colloids and Surfaces B: Biointerfaces 10, 365-377.

Yoon, J.Y., Kim, K.H., Choi, S.W., Kim, J.H., Kim, W.S., 2003. Effects of surface characteristics on non-specific agglutination in latex immunoagglutination antibody assay. Colloids and Surfaces B: Biointerfaces 27, 3-9.

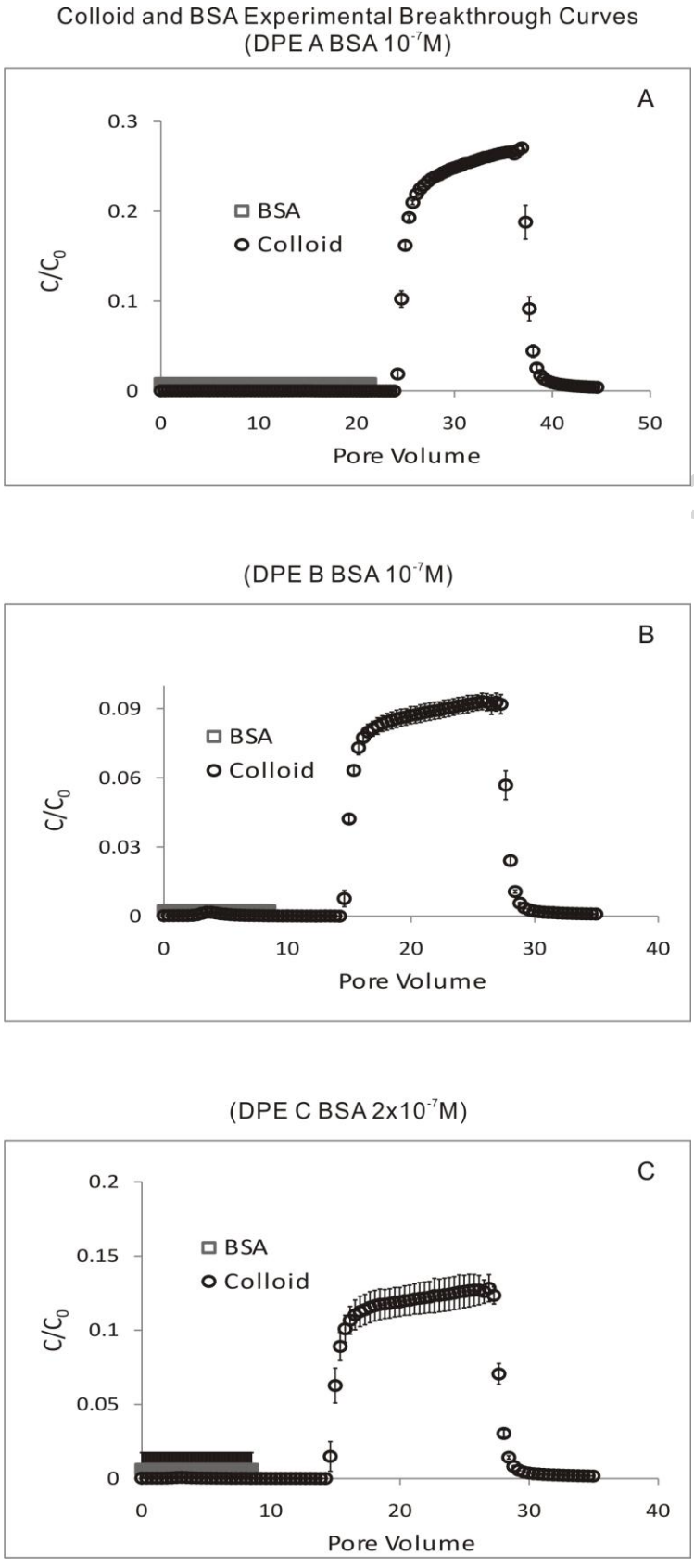

Fig. 1

Colloid and BSA Experimental Breakthrough Curves
(DPE D BSA 4×10^{-6} M)

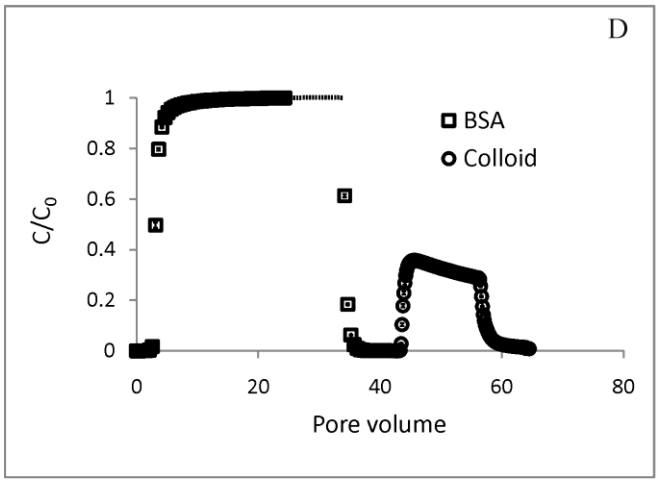

(DPE E BSA 4×10^{-6} M)

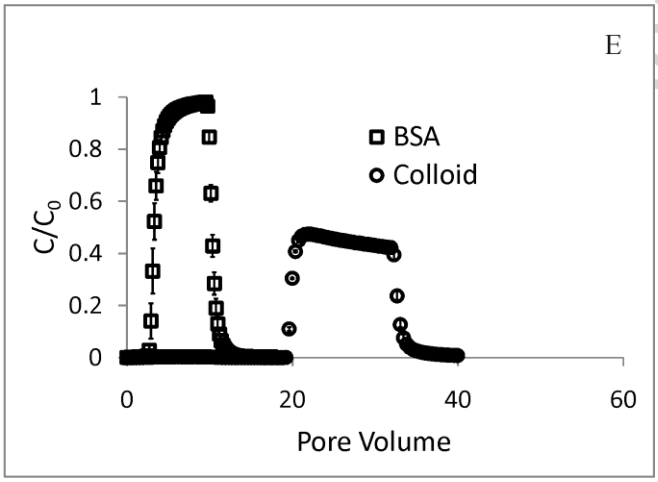

(DPE F BSA 10^{-6} M)

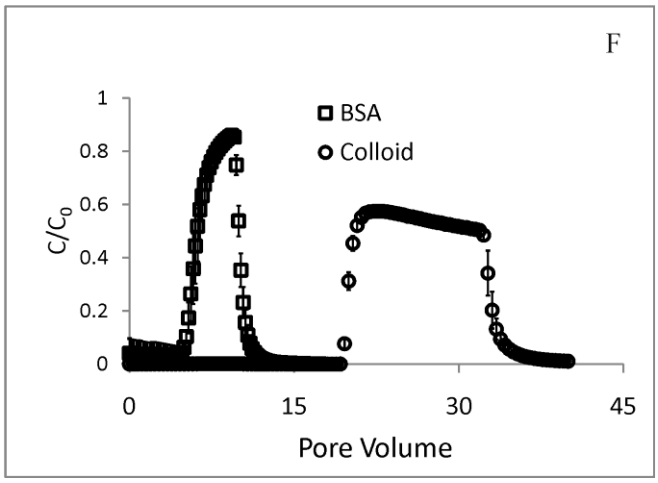

Fig. 2

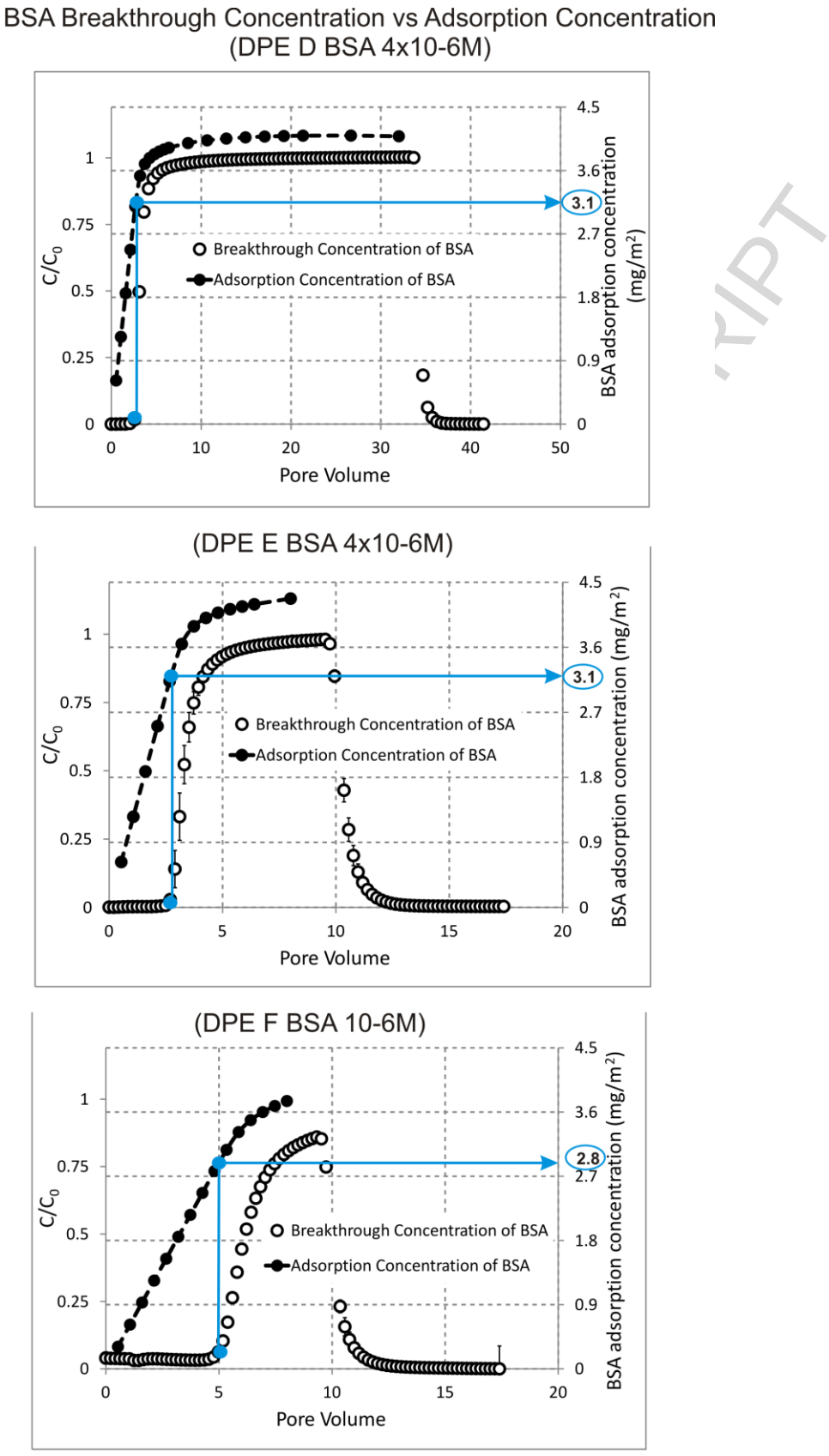

Fig. 3

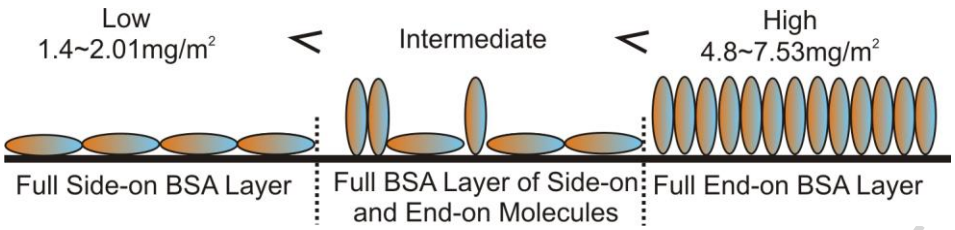

Fig. 4

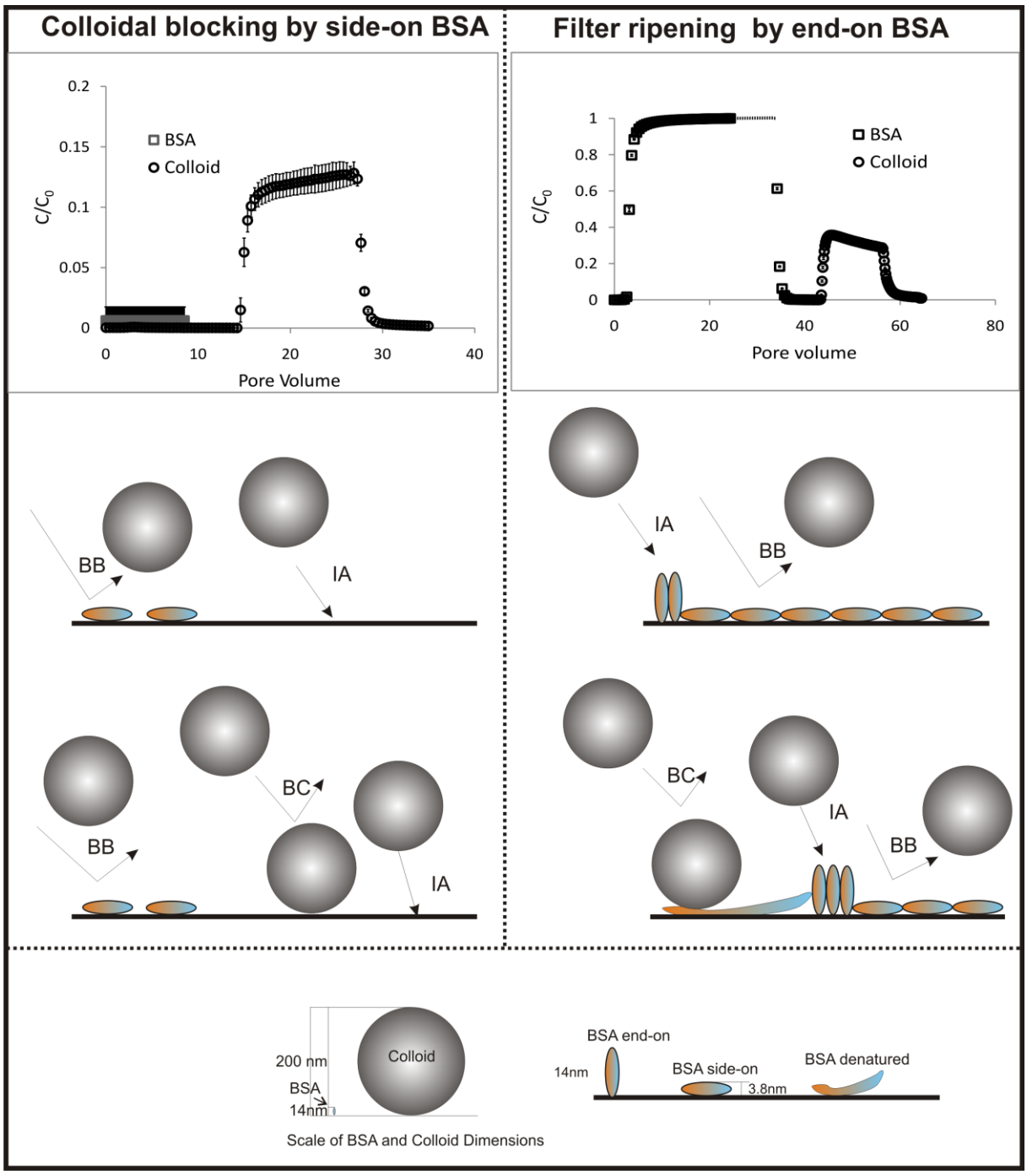

Fig. 5

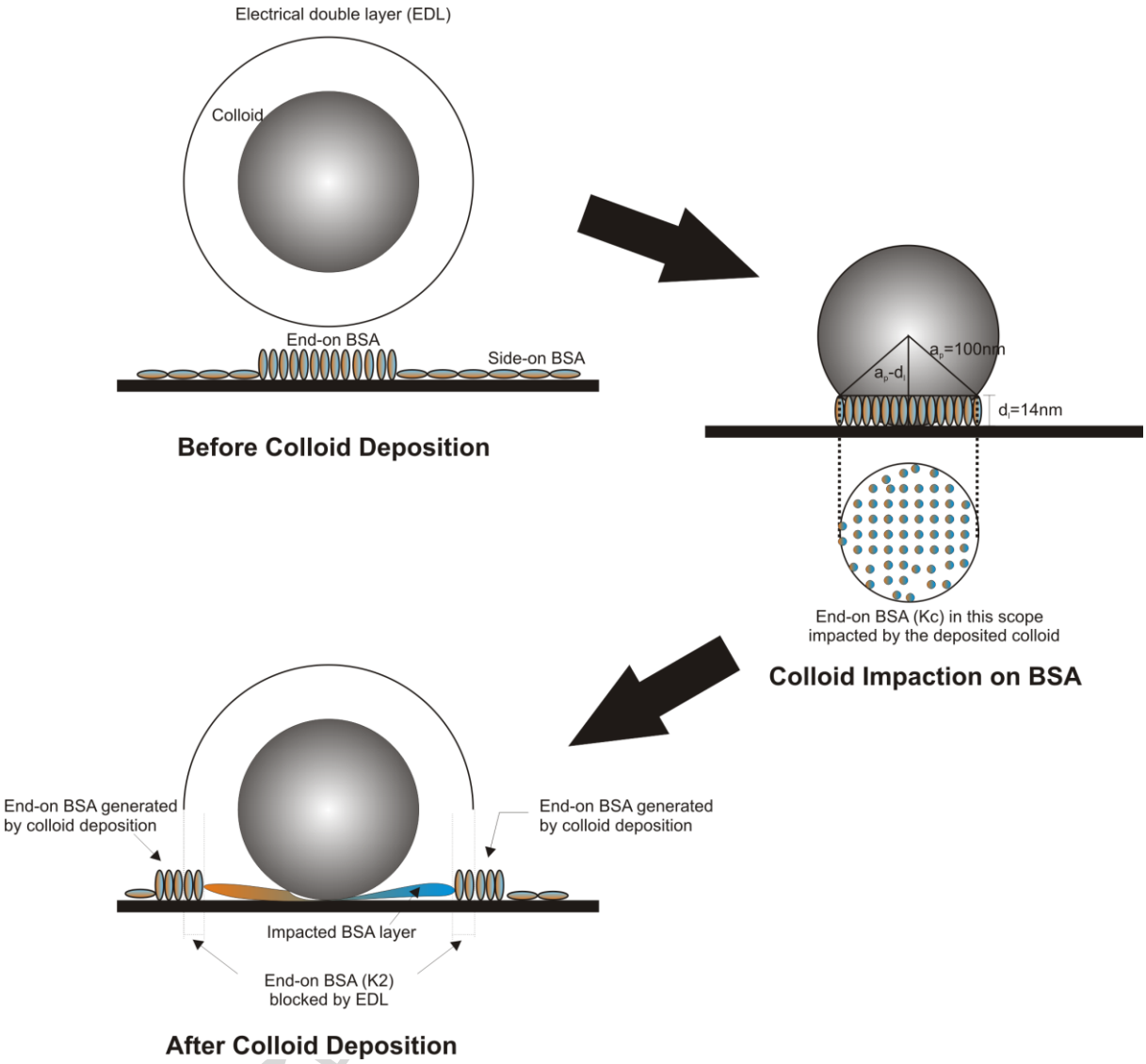

Fig. 6

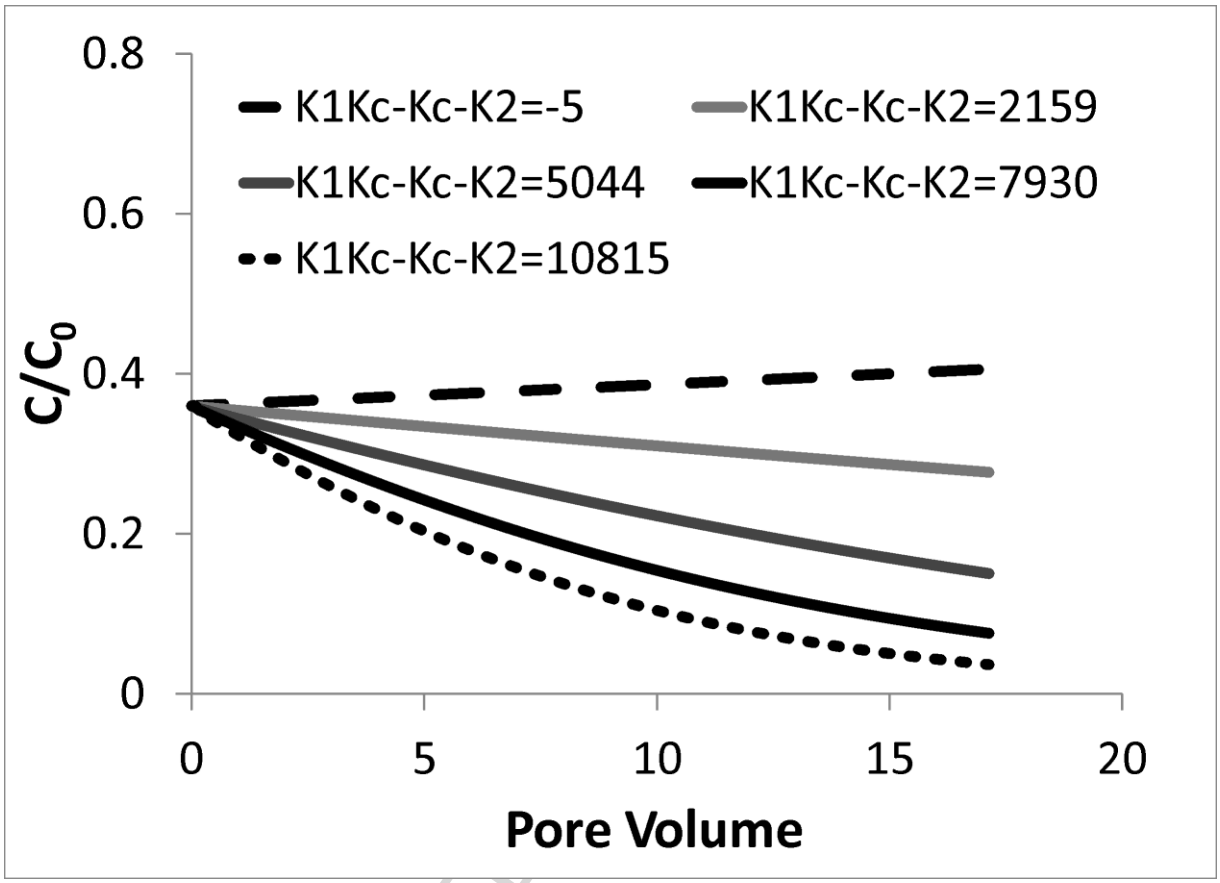

Fig. 7

Experimental and Simulated Colloid Breakthrough Curves
(DPE D BSA 4x10^{-6}M)

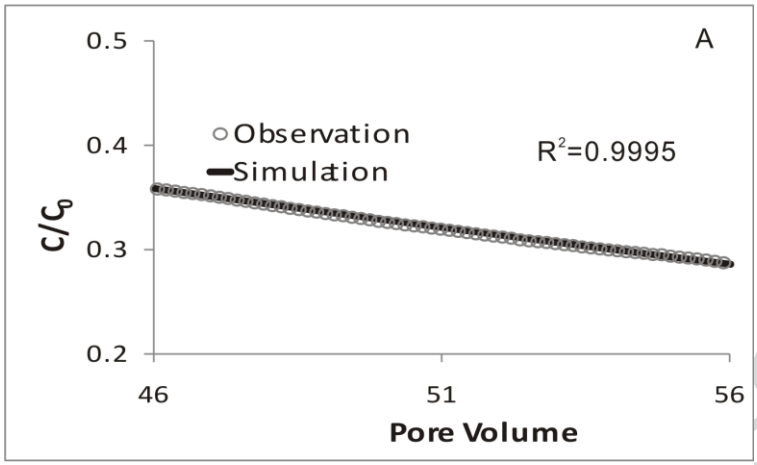

(DPE E BSA 4x10^{-6}M)

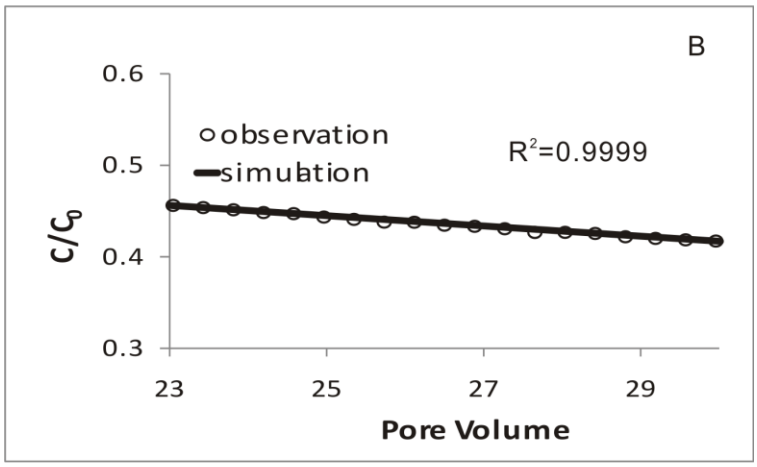

(DPE F BSA 10^{-6}M)

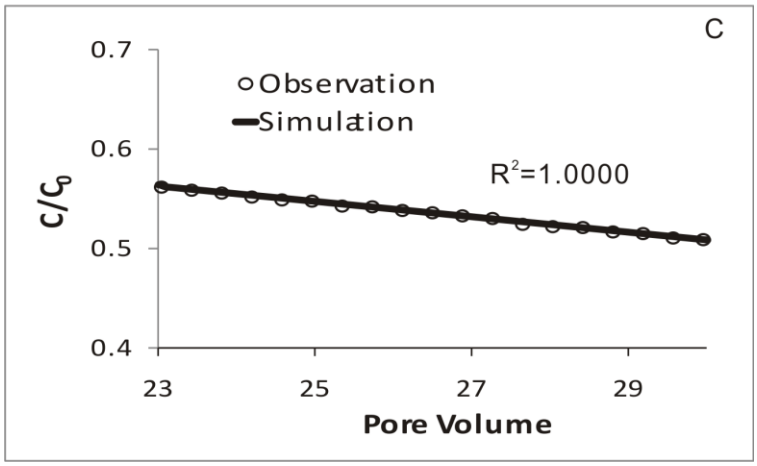

Fig. 8

Table1 List of Double Pulse Column Experiments and Adsorbed Masses

Experiment	Injection sequence	Injected BSA concentration (M)	Length of BSA pulse (PVs)	BSA adsorption concentration (mg/m^2)	Microspheres deposited in column (10^{10})*
DPE A	BSA-Microsphere	$1x10^{-7}$	13	1.15±0.00	2.23±0.01
DPE B	BSA-Microsphere	$1x10^{-7}$	3	0.29±0.00	2.72±0.01
DPE C	BSA-Microsphere	$2x10^{-7}$	3	0.58±0.00	2.62±0.03
DPE D	BSA-Microsphere	$4x10^{-6}$	32	4.09±0.04	1.94±0.01
DPE E	BSA-Microsphere	$4x10^{-6}$	8	4.33±0.57	1.61±0.05
DPE F	BSA-Microsphere	$1x10^{-6}$	8	3.91±0.11	1.31±0.04

***** All the microsphere pulses were injected at 10.4ppm for 13PVs. In the double pulse BSA-free microsphere experiments (DPE PC), microspheres deposited in the first and second pulses were $2.77±0.00×10^{10}$ and $2.71±0.01×10^{10}$, respectively.

Table 2 Model Parameters* & Results

Experiment	Fitting parameter	Model calculation		
	$K_1K_c - K_c - K_2$ ** (10^4)	$\eta_r(0)$** (10^{-3})	$\eta_r(end)$** (10^{-3})	$\Delta\eta_r/\eta_r(0)$ **
DPE D	1.12±0.01	4.73±0.04	5.95±0.1	27.0±0.5%
DPE E	1.35±0.2	3.40±0.10	4.30±0.03	26.5±0.3%
DPE F	2.01±0.02	2.53±0.05	3.46±0.17	37.0±0.5%

*Column length =0.03m; column inner diameter=0.01m; sand diameter = 0.125mm; porosity =0.39; particle diameter=200nm; particle input concentration= 10.4ppm; particle flow velocity =7.5m/day.

**$K_1K_c - K_c - K_2$=net number of end-on BSA molecules generated by one deposited particle (=generated number-deactivated number). K_1 refers to the number of end-on BSA generated due to one impacted BSA, K_c, and K_2 respectively refer to the number of end-on BSA physically impacted and electrostatically blocked by one deposited particle. The model does not calculate the value for each parameter in the expression, but estimates the total value of the expression by fitting the model output to the ripening section of the microsphere breakthrough curve. $\eta_r(0)$=initial single collector efficiency of particles; $\eta_r(end)$=single collector efficiency of particles in the end of the injection pulse; $\Delta\eta_r/\eta_r(0)$=the percentage rise in the single collector efficiency between the start and the end of the particle pulse.

Research highlights

- A conceptual model was developed to interpret colloid deposition on protein.
- Protein adsorbed in side-on conformation inhibited colloid deposition.
- Protein adsorbed in end-on conformation promoted colloid deposition.
- A mathematic model was developed to simulate colloid deposition on the protein.